

Adapting to a Changing Environment: Non-Obvious Thresholds in Multi-Scale Systems

Clare Perryman and Sebastian Wieczorek

Mathematics Research Institute, University of Exeter, EX4 4QF, UK

Many natural and technological systems fail to adapt to changing external conditions and move to a new state if the conditions vary too fast. Such “non-adiabatic” processes are ubiquitous, but little understood. We identify these processes with a new nonlinear phenomenon—an intricate *threshold* where a forced system fails to adiabatically follow a changing stable state. In systems with multiple time-scales such thresholds are generic, but non-obvious, meaning they cannot be captured by traditional stability theory. Rather, the phenomenon is organised by concepts from modern singular perturbation theory: folded singularities and canard trajectories, including *composite canards*. Thus, non-obvious thresholds should explain the failure to adapt to a changing environment in a wide range of multi-scale systems including: tipping points in the climate system, regime shifts in ecosystems, excitability in nerve cells, adaptation failure in regulatory genes, and adiabatic switching in technology.

Keywords rate-induced bifurcations, canards, folded singularity, thresholds

I. INTRODUCTION

The time evolution of real-world systems often takes place on multiple time-scales, and is paced by changing external conditions. Of particular interest are situations where, if the external conditions change too fast, the system fails to adapt and moves to a new state. In climate science and ecology one speaks of “rate-induced tipping points” [1–4], the “critical rate hypothesis” [5], and “adaptation failure” [6] to describe sudden transitions caused by too rapid changes in external conditions (e.g. dry and hot climate anomalies or wet periods due to El Niño-Southern Oscillation). In neuroscience, type III excitable nerves [7, Ch. 7] accommodate slow changes in an externally applied voltage, but an excitation requires a rapid enough increase in the voltage [8, 9]. However, such rate-induced transitions cannot be explained by classical stability theory, and require an alternative approach.

This paper conceptualises the failure to adapt to a changing environment as

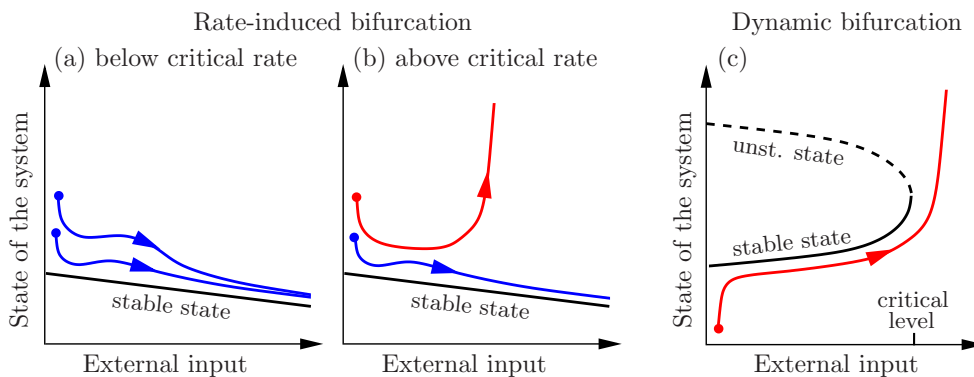


FIG. 1: (Colour online) The conceptual difference between (a)–(b) a rate-induced bifurcation and (c) a dynamic bifurcation in systems with a time-varying external input. The “stable state” is an asymptotic stable state when the external input is fixed in time. In (a)–(b), a response to a varying external input is (red) non-adiabatic, meaning the system destabilises, or (blue) adiabatic, meaning the system tracks the moving stable state.

a *rate-induced bifurcation* [1, 10]— a non-autonomous instability characterised by *critical rates* of external forcing [1, 10] and *instability thresholds* [1, 11]. Rate-induced bifurcations can be counter-intuitive because they occur in systems where a stable state exists continuously for all fixed values of the external input [Fig. 1(a)–(b)]. When the external input varies in time, the position of the stable state changes and the system tries to keep pace with the changes. The forced system *adiabatically follows* or *tracks* the continuously changing stable state if the external input varies slowly enough [Fig. 1(a)]. However, many systems fail to track the changing stable state if the external input varies too fast. These systems have initial states that destabilise—move away to a new, distant state—above some critical rate of forcing [Fig. 1(b)]. This happens even though there is no obvious loss of stability. Moreover, in systems with multiple time-scales there may be no obvious threshold separating the adiabatic and non-adiabatic responses in Fig. 1(b). This is in contrast to dynamic bifurcations [12], which can be explained by classical bifurcations of the stable state at some critical level of external input [Fig. 1(c)]. In this case, the forced system destabilises totally predictably around the critical level, independently of the initial state and of the rate of change.

In the absence of an obvious threshold, scientists are often puzzled by the

actual boundary separating initial states that adapt to changing external conditions from those that fail to adapt. The first non-obvious threshold was identified only recently, in the context of a rate-induced climate tipping point termed the “compost-bomb instability”, as a *folded saddle canard* [1]. This finding explained a sudden release of soil carbon from peat lands into the atmosphere above some critical rate of warming, which puzzled climate carbon-cycle scientists [1, 13]. Subsequently, similar non-obvious “firing thresholds” explained the spiking behaviour of type III neurons [11, 14].

Here, we discuss different types of non-obvious thresholds and reveal a threshold type with an intricate band structure. The uncovered threshold is generic, and should explain the failure to adapt to a changing environment in a wide range of nonlinear multi-scale systems. Specifically, the intricate band structure is shown to arise from a combination of the complicated dynamics due to a folded node singularity [15] and the simple threshold behaviour due to a folded saddle singularity [1] near a type I folded saddle-node [16–18]. What is more, the threshold is identified with special *composite canards*—trajectories that follow canard segments of different folded singularities. More generally, we discuss our contribution in the context of previous results from canard theory and its applications.

II. A GENERAL FRAMEWORK FOR NON-OBVIOUS THRESHOLDS

Our general framework is based on geometric singular perturbation theory [19, 20]. It builds on the ideas developed in [1], and extends the analysis to a general forcing type. Specifically, we consider multi-scale dynamical systems akin to simple climate, neuron, and electrical circuit models [1, 11, 13, 14, 21–23]:

$$\delta \, dx/dt = f(x, y, \lambda(\epsilon t), \delta), \quad (1)$$

$$dy/dt = g(x, y, \lambda(\epsilon t), \delta), \quad (2)$$

with a fast variable x , slow variable y , sufficiently smooth functions f and g , and a small parameter $0 < \delta \ll 1$. The time-varying external input $\lambda(\epsilon t)$ evolves on

a slow time-scale

$$\tau = \epsilon t,$$

and remains between λ_{\min} and λ_{\max} .

When λ does not vary in time, i.e. when $\epsilon = 0$, Eqs. (1)–(2) define a dynamical system with one fast and one slow variable, and a parameter λ . In the singular limit $\delta = 0$, the slow subsystem $dy/dt = g(x, y, \lambda, 0)$ evolves on the one-dimensional critical manifold $S(\lambda)$, defined by $f(x, y, \lambda, 0) = 0$. Alternatively, $S(\lambda)$ consists of steady states of the fast subsystem $dx/dT = f(x, y, \lambda, 0)$, where $T = t/\delta$ is the fast time-scale, and y acts as a second parameter. The critical manifold can have an attracting part $S^a(\lambda)$ and a repelling part $S^r(\lambda)$, which are separated by a fold point $F(\lambda)$ tangent to the fast x direction (Fig. 2). To give precise statements about non-obvious thresholds we assume for every fixed λ between λ_{\min} and λ_{\max} :

(A1) *The system has a quadratic nonlinearity.* The critical manifold $S(\lambda)$ is locally a graph over x with a single fold $F(\lambda)$ tangent to the fast x direction, defined by

$$\partial f / \partial x = 0 \quad \text{and} \quad \partial^2 f / \partial x^2 \neq 0. \quad (3)$$

(A2) *The system is stable for all fixed external conditions.* Near $F(\lambda)$, $S^a(\lambda)$ contains just one steady state $\tilde{x}(\lambda)$ which is asymptotically stable and varies continuously with λ .

The geometric structure of the phase space in the singular limit $\delta = 0$ gives insight into the dynamics for δ small, but nonzero. Specifically, for $0 < \delta \ll 1$, where the steady states of the fast subsystem are hyperbolic (i.e. on $S^a(\lambda)$ and $S^r(\lambda)$, but not on F), system (1)–(2) has a slow attracting manifold $S_\delta^a(\lambda)$ and a slow repelling manifold $S_\delta^r(\lambda)$, which are locally invariant, lie close to, and have the same stability type as $S^a(\lambda)$ and $S^r(\lambda)$, respectively [19, 20].

When λ varies smoothly in time such that $0 < \epsilon \lesssim 1$ and $0 < \delta \ll \epsilon$, Eqs. (1)–(2) define a dynamical system with one fast and two slow variables:

$$\delta \epsilon \, dx/d\tau = f(x, y, \lambda(\tau), \delta), \quad (4)$$

$$\epsilon \, dy/d\tau = g(x, y, \lambda(\tau), \delta), \quad (5)$$

$$d\tau/d\tau = 1. \quad (6)$$

Then the critical manifolds S^a and S^r , as well as the slow manifolds S_δ^a and S_δ^r are two-dimensional, and \tilde{x} and F form curves (Fig. 2). When $\lambda(\epsilon t)$ varies slowly enough, the forced system (1)–(2) tracks the continuously changing stable state $\tilde{x}(\lambda(\epsilon t))$. However, sometimes it may fail to track. For a given initial state, we say that system (1)–(2) *destabilises* if the trajectory crosses F and moves away from \tilde{x} along the fast x direction. The trajectory may eventually return to S_δ^a in an (monostable) excitable system [1, 11], or approach a different state in a multistable system. We define the *critical rate* ϵ_c as the smallest ϵ above which there are initial states in S_δ^a that destabilise. Then we define the *instability threshold* as the boundary within S_δ^a separating initial states that track $\tilde{x}(\lambda(\epsilon t))$ from those that destabilise.

Figure 2 (a)–(b) shows two trajectories of Eqs. (1)–(2) for different initial states on S^a . Below the critical rate, all trajectories track, and eventually converge to $\tilde{x}(\lambda(\epsilon t))$ [Fig. 2(a)]. However, above the critical rate there are initial states near \tilde{x} that fail to track $\tilde{x}(\lambda(\epsilon t))$, and destabilise [Fig. 2(b)]. The two qualitatively different behaviours in Fig. 2(b) show there is an instability threshold within S_δ^a . What is more, this threshold can be simple [Fig. 2(c)] as reported in [1, 11], or can have an intriguing band structure [Fig. 2(d)] that has not been reported to date. In both cases, it is not immediately obvious what determines such thresholds.

We set $\delta = 0$ to identify the dynamical mechanism for non-obvious thresholds. System (4)–(6) is reduced to the slow dynamics on S , and projected onto the (x, τ) -plane by differentiating Eq. (4) with respect to slow time τ :

$$dx/d\tau = -\frac{g \partial f / \partial y + (\partial f / \partial \lambda)(d\lambda/dt)}{\epsilon \partial f / \partial x} \Big|_S, \quad (7)$$

$$d\tau/d\tau = 1. \quad (8)$$

It now becomes clear that if a trajectory deviates too much from \tilde{x} and approaches a typical point on F , then $\partial f / \partial x$ in Eq. (7) approaches zero, and x diverges off to infinity in finite slow time τ . However, there may be special points on F where

$$[g \partial f / \partial y + (\partial f / \partial \lambda)(d\lambda/dt)]|_F = 0, \quad (9)$$

so $dx/d\tau$ remains finite. Such special points are referred to as *folded singularities* [15, 24]. The corresponding trajectories, that cross from S^a along the

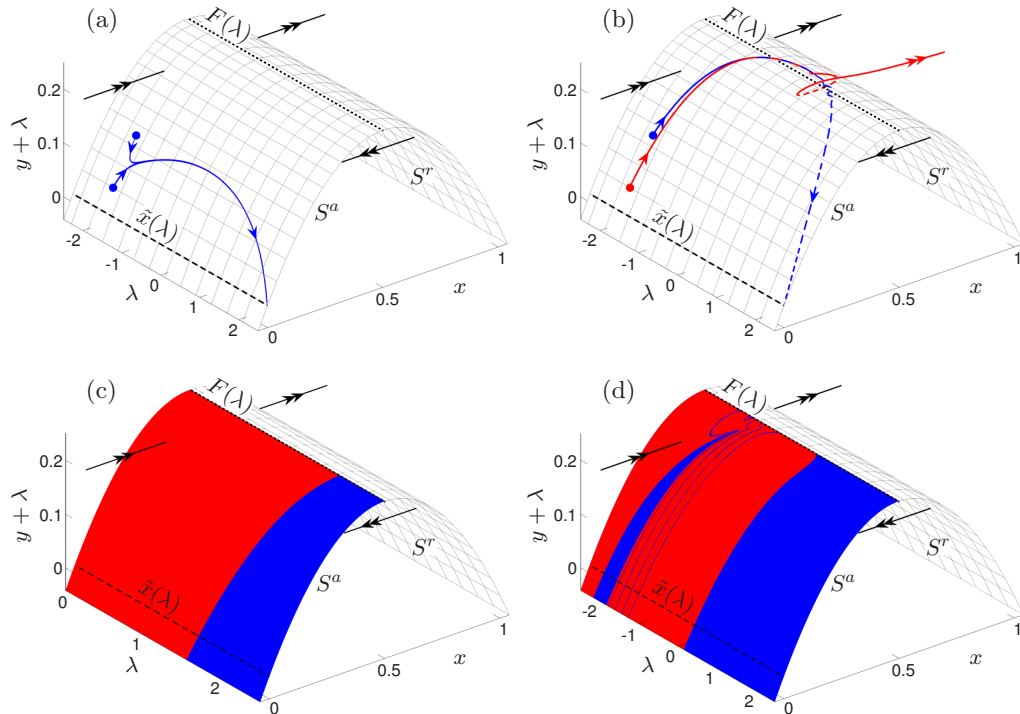


FIG. 2: (Colour online) (a)–(b) Trajectories starting at two different initial states (dots) on S^a , near the changing stable state \tilde{x} , (a) below and (b) above the critical rate. (c)–(d) Above the critical rate, initial states on S^a that (red) destabilise or (blue) track $\tilde{x}(\lambda(\epsilon t))$ highlight different threshold types. We used Eqs. (1)–(2), (13), and [(a), (b), (d)] Eq. (14) with (a) $\epsilon = 0.06$ and [(b), (d)] $\epsilon = 0.216$; and (c) Eq. (15) with $\epsilon = 1$. Other parameters were $\delta = 0.01$, $\lambda_{\max} = 2.5$, and (a)–(b) $\lambda(0) = -1.7$. For (a)–(d) the critical manifold $S(\lambda)$ is given by $y = -\lambda - x(x - 1)$, has a fold $F(\lambda)$ at $(x, y) = (1/2, -\lambda + 1/4)$ and a unique stable steady state $\tilde{x}(\lambda)$ at $(x, y) = (0, -\lambda)$. For clarity, the plots are shown in the co-moving coordinate system $(x, y + \lambda, \lambda)$. The λ axis can be transformed into a slow time axis using [(a), (b), (d)] Eq. (14) or (c) Eq. (15).

eigendirections of a folded singularity onto S^r , are referred to as *singular canards* [15]. To study the flow near F , where Eqs. (7)–(8) are singular, we reverse time on S^r according to [25]:

$$d\tau = -ds \epsilon (\partial f / \partial x)|_S.$$

This gives the desingularised system

$$dx/ds = [g \partial f / \partial y + (\partial f / \partial \lambda)(d\lambda/dt)]|_S, \quad (10)$$

$$d\tau/ds = -\epsilon (\partial f / \partial x)|_S, \quad (11)$$

where folded singularities become regular steady states. One speaks of “folded

nodes”, “folded saddles” and “folded foci” for Eqs. (7)–(8) if a steady state for Eqs. (10)–(11) has real eigenvalues with the same sign, real eigenvalues with opposite signs, and complex eigenvalues with nonzero real parts, respectively. A phase portrait of Eqs. (7)–(8) is obtained by reversing the flow on S^r in the phase portrait of Eqs. (10)–(11). Finally, for $0 < \delta \ll 1$, key singular canards for (7)–(8) perturb to *maximal canards* in (4)–(6) which are formed by transverse (hence robust) intersections of the attracting S_δ^a and repelling S_δ^r slow manifolds [15, 26, 27]. Such intersections are possible in system (4)–(6) because the slow manifolds S_δ^a and S_δ^r are two-dimensional, and can be extended across the fold. Here, we show maximal canards γ_δ in Fig. 4, and their approximations by singular canards γ in Figs. 3 and 5.

Often in real-life applications the changing external conditions λ are expressed as a prescribed function of time t , but not ϵ . Specifying ϵ in $\lambda(\epsilon t)$ is not necessary if one replaces τ with ϵt in Eqs. (4)–(11). However, ϵ is useful for defining critical rates of change.

III. EXISTENCE AND TWO CASES OF A NON-OBVIOUS THRESHOLD

Using the general framework, we can study non-obvious thresholds where multi-scale systems fail to adapt to a changing environment. Above the critical rate, the system is guaranteed to have initial states on S_δ^a that fail to track the moving stable state $\tilde{x}(\lambda(\epsilon t))$. However, the system is not guaranteed to have a threshold; for example, if all the initial states on S_δ^a destabilise, as in [10, Sec. 3(c)], there is no threshold. Results on the existence of critical rates and non-obvious thresholds are derived in detail in [28]. Here, guided by the general framework from Sec. II and the existence results below, we identify two distinct threshold types and uncover the dynamical mechanism behind the complicated threshold shown in Fig. 2(d).

Existence of critical rates: a dissipative Adiabatic Theorem. Suppose the forced system (1)–(2) with assumptions (A1)–(A2) satisfies both the folded sin-

gularity condition (9), and the non-zero speed condition

$$\left. \frac{d[g \partial f / \partial y + (\partial f / \partial \lambda)(d\lambda / dt)]|_F}{d\epsilon} \right|_F \neq 0 \quad (12)$$

at the same time t . Then (1)–(2) has a critical rate ϵ_c .

Existence of non-obvious thresholds. An instability threshold in the forced system (1)–(2) with assumptions (A1)–(A2) requires a folded saddle singularity within $(\lambda_{\min}, \lambda_{\max})$. The system is guaranteed to have an instability threshold if a folded saddle is the only folded singularity.

An analysis of the phase portraits satisfying (A1)–(A2) and containing a folded saddle reveals two cases of a non-obvious threshold [28]. Which case occurs depends on both the system (1)–(2), and the forcing $\lambda(\epsilon t)$. What is more, different cases can occur for the same system when subject to different $\lambda(\epsilon t)$. We illustrate these two cases of a non-obvious threshold using an example of (1)–(2) with

$$f = x(x - 1) + y + \lambda(\epsilon t) \quad \text{and} \quad g = -x, \quad (13)$$

and two different forcing functions $\lambda(\epsilon t)$.

Case 1: Complicated threshold due to a type I folded saddle-node singularity. Consider example (13) subject to logistic growth at a rate ϵ :

$$\lambda(\epsilon t) = \lambda_{\max} \tanh(\epsilon t - c), \quad (14)$$

where $\lambda \in (-\lambda_{\max}, \lambda_{\max})$ and

$$c = \tanh^{-1}(\lambda(0)/\lambda_{\max}).$$

It follows from Eqs. (10)–(14) that, upon increasing ϵ , a type I folded saddle-node appears within $(-\lambda_{\max}, \lambda_{\max})$ at $\epsilon = (2\lambda_{\max})^{-1}$, which is approximately the critical rate ϵ_c for $0 < \delta \ll 1$. The ensuing saddle-node bifurcation of folded singularities gives rise to a folded node (focus) $FN(FF)$ at $(x, \lambda) = (1/2, -\sqrt{\lambda_{\max}(\lambda_{\max} - (2\epsilon)^{-1})})$ and a folded saddle FS at $(x, \lambda) = (1/2, \sqrt{\lambda_{\max}(\lambda_{\max} - (2\epsilon)^{-1})})$. The presence of a folded saddle means there may be an instability threshold. Figure 3 shows that there is one indeed for $0 < \delta \ll 1$. The instability threshold is defined on the stable slow manifold S_δ^a which is difficult to compute near the fold F . To facilitate the computations, we consider initial states on the critical manifold S^a , which is known exactly. Away from F ,

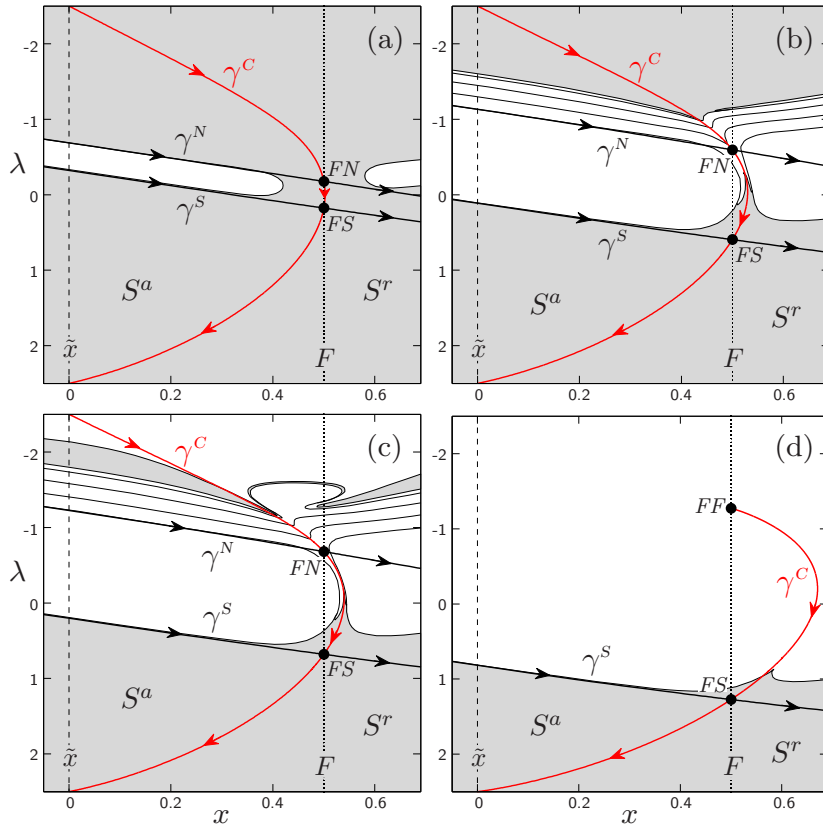


FIG. 3: (Colour online) Initial states on the critical manifold S that (white) destabilise or (grey) track $\tilde{x}(\lambda(\epsilon t))$ in Eqs. (1)–(2) and (13)–(14) with $\delta = 0.01$, $\lambda_{\max} = 2.5$, and $\epsilon =$ (a) 0.201, (b) 0.212, (c) 0.216, and (d) 0.270, shown projected onto the (x, λ) plane. Away from F , the instability threshold in S_δ^a is well approximated by the white-grey boundary in S^a . Points FN , FS , and FF are folded node, folded saddle, and folded focus singularities, respectively; the strong folded node singular canard γ^N and the folded saddle singular canard γ^S approximate projections of the maximal canards γ_δ^N and γ_δ^S , respectively, onto S . The projection of the maximal canard γ_δ^C onto S is approximated by the weak folded node/faux saddle singular canard γ^C when $\lambda > -1$, but lies below γ^C for $-2.5 < \lambda < -1$, e.g. within the wide grey band around $\lambda = -2$ in (c). Compare (c) with Fig. 2(d).

the critical manifold S^a closely approximates the slow manifold S_δ^a . Here, the threshold is well approximated by the boundaries between the white and grey regions. However, caution is required near F , especially around FN , where S_δ^a twists in a complicated manner [27, Fig.6], and the chosen surface of initial conditions, S^a , intersects these twists. There, the boundaries between the white and grey regions deviate from the threshold due to the choice of initial states. We

also show what happens to initial states on S^r just to the right of F , as some are mapped along the fast flow onto S_δ^a and converge to \tilde{x} . This is why a “reflection” of the band structure from S^a can be seen on S^r .

Shortly past the saddle-node bifurcation, there are three bands of initial states on S_δ^a [Fig. 3(a)]. The threshold separating the bands is given by two maximal canards. The folded saddle maximal canard γ_δ^S and the strong folded node maximal canard γ_δ^N enclose a narrow (white) band of initial states from which trajectories move directly towards F , then cross F and destabilise—move away from \tilde{x} along the fast x -direction. Trajectories from the grey band on S^a and below γ_δ^S approach γ_δ^C and thereby converge to \tilde{x} . This is in contrast to trajectories from the grey band on S^a and above γ_δ^N . These trajectories initially approach and twist around γ_δ^C , and also cross F . However, rather than destabilising, they are fed back along γ_δ^C onto the stable slow manifold, and eventually converge to \tilde{x} [Fig. 2(b), blue trajectory]. Finally, grey and white initial states on S^r are mapped along the fast flow onto the grey and white, respectively, bands of S_δ^a .

As ϵ increases, the threshold becomes more complicated due to the presence of the folded node FN . Additional threshold curves appear successively above γ_δ^N , giving five white bands of initial states that destabilise in Fig. 3(b). Trajectories started within these additional white bands twist around γ_δ^C before destabilising, [Fig. 2(b), red trajectory]. The white bands have black boundaries and are separated by thin grey bands which are difficult to see in Fig. 3; see the thin grey band in the inset of Fig. 4, or thin blue bands in Fig. 2(d). Trajectories started within these thin grey bands follow a maximal canard on S_δ^r for some time, but then return to S_δ^a into the region below γ_δ^S , and converge to \tilde{x} . The white bands expand with ϵ and approach the weak folded node maximal canard γ_δ^C on both sides [Fig. 3(c)]. When the folded node FN turns into a folded focus FF at $\epsilon = (2 + \sqrt{4 + \lambda_{\max}^2})/8\lambda_{\max}$, its canards disappear [15] and so does the band structure [Fig. 3(d)]. We are left with a simple threshold, given just by γ_δ^S [14].

The key mechanism for complicated thresholds is the phenomenon whereby trajectories leave S_δ^a through the folded node region and are fed back to S_δ^a through the folded saddle region. This phenomenon has two consequences. Firstly, not all initial states on S_δ^a and above γ_δ^N destabilise. Secondly, the initial states on S_δ^a that destabilise or track \tilde{x} form alternating bands, and these bands

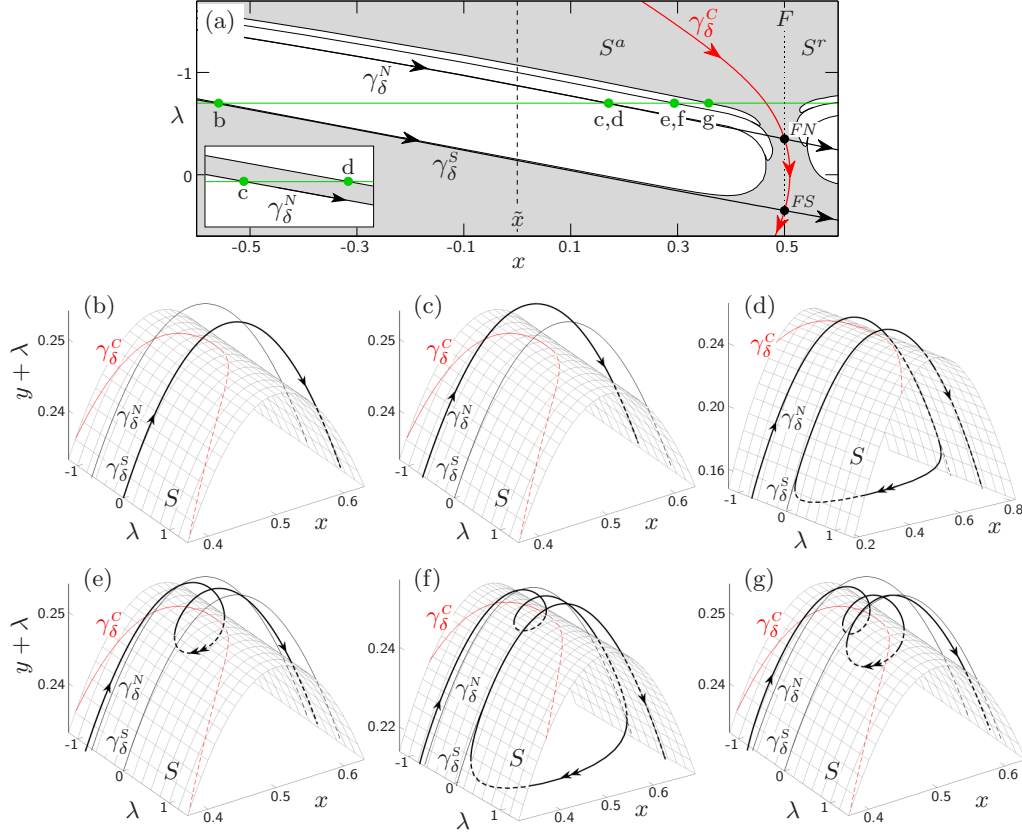


FIG. 4: (Colour online) (a) Initial states on the critical manifold S that (white) destabilise or (grey) track $\tilde{x}(\lambda(\epsilon t))$ in Eqs. (1)–(2) and (13)–(14) with $\delta = 0.01$ and $\epsilon = 0.204$. Inset shows grey band between c and d ; a similar band exists between e and f . Labels b – g for $\lambda(0) = -0.7$ denote different threshold components including: (b) the folded saddle maximal canard γ_δ^S , (c) the strong folded node maximal canard γ_δ^N , (d) a composite canard that follows γ_δ^N and γ_δ^S , (e) a secondary folded node maximal canard, (f) a composite canard that follows a secondary maximal canard and γ_δ^S , (g) a secondary folded node maximal canard.

have not been identified before. To be more specific, the white bands are related to the known rotational sectors of a folded node. However, whilst rotational sectors are separated by a single trajectory, the maximal canard [26, 27], our white bands are separated by a narrow grey band. Each grey band is bounded by two different canards.

Figure 4 identifies different components of the complicated threshold. They consist of known maximal canards such as (b) γ_δ^S , (c) γ_δ^N , and [(e) and (g)] secondary folded node maximal canards that bifurcate off γ_δ^C [26]. These canards form the lower boundaries of the narrow grey bands. Most interestingly,

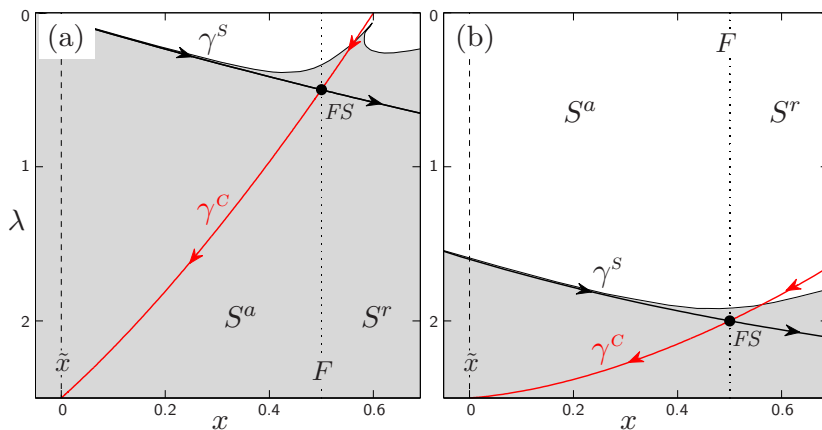


FIG. 5: (Colour online) Initial states on the critical manifold S that (white) destabilise or (grey) track $\tilde{x}(\lambda(\epsilon t))$ for Eqs. (1)–(2), (13), and (15) with $\delta = 0.01$, $\lambda_{\max} = 2.5$, and (a) $\epsilon = 0.25$, (b) $\epsilon = 1$, shown projected onto the (x, λ) plane. Away from F the instability threshold in S^g is well approximated by the white-grey boundary in S^a . Compare (b) with Fig. 2(c). For labels see Fig. 3.

we uncover *composite canards* that follow canard segments of different folded singularities. These canards form the upper boundaries of the narrow grey bands. Figure 4 shows composite canards which initially (d) follow γ_δ^N , or (f) follow the first secondary folded node maximal canard, and then [(d) and (f)] follow γ_δ^S . This explains the intriguing band structure with intermingled regions of white and grey in Figs. 3(b)–(c) and 4(a), or red and blue in Fig. 2(d). It is interesting to note, the composite canards in Fig. 4(d) and (f) are reminiscent of trajectories that switch between different primary and secondary canards of the same folded node in a stellate cell model [29].

Case 2: Simple threshold due to an isolated folded saddle singularity. Consider example (13) subject to an exponential approach at a rate ϵ :

$$\lambda(\epsilon t) = \lambda_{\max} (1 - c e^{-\epsilon t}), \quad (15)$$

where $\lambda \in (0, \lambda_{\max})$ and

$$c = 1 - \lambda(0)/\lambda_{\max}.$$

It follows from Eqs. (10)–(13) and (15) that, upon increasing ϵ , an isolated folded saddle FS at $(x, \lambda) = (1/2, \lambda_{\max} - (2\epsilon)^{-1})$ enters $(0, \lambda_{\max})$ via its lower boundary at $\epsilon = (2\lambda_{\max})^{-1}$, which is approximately the critical rate ϵ_c for $0 < \delta \ll 1$.

Hence, there is an instability threshold. Figure 5 shows the threshold is given by the folded saddle maximal canard γ_δ^S , as in the compost-bomb and the type III neuron examples [1, 11]. Note, this threshold is very similar to that in Fig. 3(d).

IV. CONCLUSIONS

In summary, we analysed multiple time-scale systems subject to a changing environment, and identified nonlinear mechanisms for the failure to adapt. Specifically, we described thresholds where a system fails to adiabatically follow a continuously changing stable state. Despite their cross-disciplinary nature, these thresholds are largely unexplored because they are “non-obvious”, meaning they cannot, in general, be revealed by traditional stability theory. Thus, they require an alternative approach. We presented a framework, based on geometric singular perturbation theory, that led us to a novel threshold type with an intriguing band structure. There are alternating bands, where trajectories track the moving stable state, or destabilise. We showed this structure is organised by a type I folded saddle-node singularity. Intuitively, it arises from an interplay of the complicated dynamics of twisting canard trajectories due to a folded node singularity, and the simple threshold behaviour illustrated for a folded saddle singularity. Most importantly, trajectories which leave the attracting slow manifold through the folded node region can be fed back to the attracting slow manifold through the folded saddle region. In more technical terms, the band structure is related to the rotational sectors of a folded node, but also differs from them in one key aspect. Whereas the rotational sectors are separated by a single trajectory, the maximal canard [26, 27], the corresponding wide bands are separated by a narrow band. These narrow bands are bounded by two different canards. One of the bounding canards is a known maximal canard, but the other is a composite canard that follows canard segments of different folded singularities. The supporting analytical theory of a type I folded saddle-node is being developed in [18].

Whilst non-obvious thresholds can be complicated, they are generic, and should explain counter-intuitive responses to a changing environment in a wide range of multi-scale systems. We highlighted their importance by examples

of climate and ecosystems failing to adapt to a rapidly changing environment [1, 10, 13], and type III excitable cells “firing” only if the voltage stimulus rises fast enough [8, 11]. More generally, our results give new insight into non-adiabatic processes in multi-scale dissipative systems, and should stimulate further work in canard theory.

Acknowledgements

We would like thank M. Wechselberger for useful discussions. The research of C.P. was supported by the EPSRC and the MCRN (via NSF grant DMS-0940363).

-
- [1] Wieczorek S, Ashwin P, Luke CM, Cox PM. 2010 Excitability in ramped systems: the compost-bomb instability. *Proc. R. Soc. A* **467**, 1243–1269. (doi:10.1098/rspa.2010.0485)
 - [2] Lenton T, Held H, Kriegler E, Hall J, Lucht W, Rahmstorf S, Schellnhuber H. 2008 Tipping elements in the Earth’s climate system. *PNAS* **105**, 1786–1793. (doi:10.1073/pnas.0705414105)
 - [3] Stocker TF, Schmittner A. 1997 Influence of CO2 emission rates on the stability of the thermohaline circulation. *Nature* **388**, 862–865.
 - [4] Leemans R, Eickhout B. 2004 Another reason for concern: regional and global impacts on ecosystems for different levels of climate change. *Global Environ Change* **14**, 219–228. (doi:10.1016/j.gloenvcha.2004.04.009)
 - [5] Scheffer M, van Nes E, Holmgren M, Hughes T. 2008 Pulse-driven loss of top-down control: the critical-rate hypothesis. *Ecosystems* **11**, 226–237. (doi:10.1007/s10021-007-9118-8)
 - [6] Bridle JR, Vines TH. 2007 Limits to evolution at range margins: when and why does adaptation fail? *Trends Ecol. Evol.* **22**, 140–147. (doi:10.1016/j.tree.2006.11.002)
 - [7] Izhikevich E. 2007 *Dynamical Systems in Neuroscience*. Computational Neuroscience. MIT Press.
 - [8] Hill AV. 1936 Excitation and accommodation in nerve. *Proc. R. Soc. Lond. B* **119**, 305–355. (doi:10.1098/rspb.1936.0012)
 - [9] Biktashev VN. 2002 Dissipation of the excitation wave fronts. *Phys. Rev. Lett.* **89**, 168102. (doi:10.1103/PhysRevLett.89.168102)

- [10] Ashwin P, Wieczorek S, Vitolo R, Cox PM. 2012 Tipping points in open systems: bifurcation, noise-induced and rate-dependent examples in the climate system. *Phil. Trans. R. Soc. A* **370**, 1166–1184. (doi:10.1098/rsta.2011.0306)
- [11] Mitry J, McCarthy M, Kopell N, Wechselberger M. 2013 Excitable neurons, firing threshold manifolds and canards. *J. Math. Neuro.* **3**, 12. (doi:10.1186/2190-8567-3-12)
- [12] Benoît E. (ed) 1991 *Dynamic Bifurcations*. Lecture Notes in Mathematics, vol. 1493. Berlin, Germany: Springer.
- [13] Luke CM, Cox PM. 2011 Soil carbon and climate change: from the Jenkinson effect to the compost-bomb instability. *Eur. J. Soil Sci.* **62**, 5–12. (doi:10.1111/j.1365-2389.2010.01312.x)
- [14] Wechselberger M, Mitry J, Rinzel J. 2013 Canard theory and excitability. In *Nonautonomous Dynamical Systems in the Life Sciences*, (eds PE Kloeden, C Poetzsche) pp. 89–132. Lecture Notes in Mathematics, vol. 2102. Springer International Publishing. (doi:10.1007/978-3-319-03080-7_3)
- [15] Szmolyan P, Wechselberger M. 2001 Canards in \mathbb{R}^3 . *J. of Diff. Eqn.* **177**, 419–453. (doi:10.1006/jdeq.2001.4001)
- [16] Krupa M, Wechselberger M. 2010 Local analysis near a folded saddle-node singularity. *J. Diff. Eqn.* **248**, 2841–2888. (doi:10.1016/j.jde.2010.02.006)
- [17] Guckenheimer J. 2008 Return maps of folded nodes and folded saddle-nodes. *Chaos* **18**, 015108. (doi:10.1063/1.2790372)
- [18] Vo T, Wechselberger M. Canards of folded saddle-node type. In preparation.
- [19] Fenichel N. 1979 Geometric singular perturbation theory for ordinary differential equations. *J. Diff. Eqn.* **31**, 53–98. (doi:10.1016/0022-0396(79)90152-9)
- [20] Jones C. 1995 Geometric singular perturbation theory. In *Dynamical Systems*, (ed R Johnson) pp. 44–118. Lecture Notes in Mathematics, vol. 1609. Berlin, Germany: Springer. (doi:10.1007/BFb0095239)
- [21] Roberts A, Widiasih E, Jones CKRT, Wechselberger M. Mixed mode oscillations in a conceptual climate model. 2013. arXiv:1311.5182.
- [22] Cessi P. 1994 A simple box model of stochastically forced thermohaline flow. *J. Phys. Oceanogr.* **24**, 1911–1920. (doi:10.1175/1520-0485(1994)024<1911:ASBMOS>2.0.CO;2)
- [23] van der Pol B. 1934 The nonlinear theory of electric oscillations. *Proc. IRE* **22**, 1051–1086. (doi:10.1109/JRPROC.1934.226781)
- [24] Takens F. 1976 Constrained equations; a study of implicit differential equations and their discontinuous solutions. In *Structural Stability, the Theory of Catastrophes, and Applications in the Sciences*, (ed P Hilton) pp. 143–234. Lecture Notes

- in Mathematics, vol. 525. Berlin, Germany: Springer. (doi:10.1007/BFb0077850)
- [25] Dumortier F, Roussarie RH. 1996 *Canard Cycles and Center Manifolds*. *Mem. Amer. Math. Soc.* No. 577.
- [26] Wechselberger M. 2005 Existence and bifurcations of canards in \mathbb{R}^3 in the case of a folded node. *SIAM J. App. Dy. Sys.* **4**, 101–139. (doi:10.1137/030601995)
- [27] Desroches M, Guckenheimer J, Krauskopf B, Kuehn C, Osinga HM, Wechselberger M. 2012 Mixed mode oscillations with multiple time scales. *SIAM Review* **54**, 211–288. (doi:10.1137/100791233)
- [28] Perryman C, Wieczorek S. Rate induced bifurcations. In preparation.
- [29] Wechselberger M, Weckesser W. 2009 Bifurcations of mixed-mode oscillations in a stellate cell model. *Phys. D* **238**, 1598–1614. (doi:10.1016/j.physd.2009.04.017)